Impact of PMD in Single-Receiver and Polarization-Diverse Direct-Detection Optical OFDM

Brendon J. C. Schmidt, Arthur James Lowery, *Fellow, IEEE*, and Jean Armstrong, *Senior Member, IEEE*

***Abstract*—Polarization-mode dispersion (PMD) can cause frequency-selective fading in direct-detection optical orthogonal frequency division multiplexing (DDO-OFDM) systems. In this paper, we examine the effects of this fading. We begin with an analysis of the frequency-selective fading caused by first-order PMD. We then estimate the impact of PMD in single-receiver DDO-OFDM using all-order simulations to generate outage probabilities as a function of signal-to-noise ratio (SNR) penalty. The performances of three single-receiver DDO-OFDM formats are compared and a new format that minimizes the frequency difference between the carrier and sideband is found to be more tolerant to PMD. We then introduce a DDO-OFM system that includes polarization diversity and carrier boost in the receiver. The effects of various configurations are simulated and the results suggest that a data rate of 42.7 Gb/s can be achieved within an optical bandwidth of 40 GHz, and with negligible PMD penalties.**

***Index Terms*—Chromatic dispersion, compensation, orthogonal frequency division multiplexing (OFDM), polarization-mode dispersion (PMD).**

I. Introduction

POLARIZATION-MODE DISPERSION (PMD) is a major barrier to increasing data rates in conventional high-speed long-haul optical communications. With channel rates of 40 Gb/s and higher proposed for next generation optical systems, the mean PMD in many installed links will become a significant fraction of the transmitted symbol period, and intersymbol interference will lead to significant signal degradation. Adaptive compensation schemes have been proposed [1]–[4], but for serial binary formats, the high symbol rates limit the performance that can be achieved [5], [6] or require complex receiver structures [7].

Optical orthogonal frequency division multiplexing (OFDM) has been proposed as an alternative modulation scheme [8], [9]. Some forms of optical OFDM can adaptively compensate for channel impairments such as chromatic dispersion and PMD, without prior knowledge of the channel characteristics. This is a significant advantage for reconfigurable networks as it allows for self-adaption to variations in a network's characteristics, such as variations in accumulated chromatic dispersion caused by optical circuit switching.

Manuscript received July 12, 2008; revised November 20, 2008 and January 30, 2009. Current version published July 22, 2009. This work was supported by the Australian Research Council's Discovery funding scheme (DP0772937).

The authors are with the Department of Electrical and Computer Systems Engineering, Monash University, Melbourne, Vic. 3800, Australia (e-mail: Brendon.Schmidt@eng.monash.edu.au; Arthur.Lowery@eng.monash.edu.au; Jean.Armstrong@eng.monash.edu.au).

Color versions of one or more of the figures in this paper are available online at http://ieeexplore.ieee.org.

Digital Object Identifier 10.1109/JLT.2009.2016987

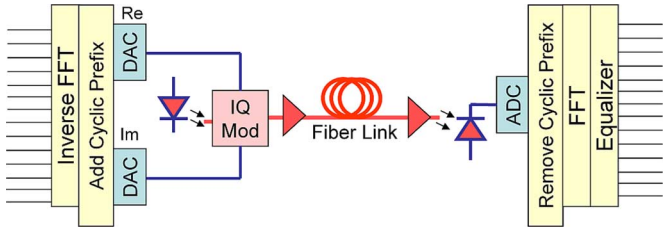

Fig. 1. Topology of the single-receiver DDO-OFDM system: DAC (digital-to-analog converter) and ADC (analog-to-digital converter).

There have been a number of demonstrations that have shown the potential of optical OFDM in long-haul optical communications. In [10] and [11], demonstrations using coherent optical OFDM (CO-OFDM) were used for the adaptive compensation of chromatic dispersion, and the effective implementation of polarization division multiplexing. Channel rates of up to 121.9 Gb/s were achieved with a spectral efficiency of 2 b/s/Hz [10]. However, this high performance came with the cost and complexity associated with coherent polarization-diverse reception. Although phase noise compensation techniques [12] have reduced the laser line width requirements associated with some implementations of CO-OFDM, a more compact and cost effective alternative would be attractive.

Direct-detection optical OFDM (DDO-OFDM) allows far simpler receiver architectures and is insensitive to laser phase noise. Although there is some loss in sensitivity [13], demonstrations have reported channel rates of up to 20 Gb/s [14], and simulations show that high levels of chromatic dispersion can be compensated for with minimal overheads [8]. DDO-OFDM has been proposed for the compensation of PMD. However, for single-receiver implementations, the frequency-selective fading caused by PMD will lead to reduced electrical signal-to-noise ratios (SNRs) in affected subcarriers [15]–[17].

In this paper, we investigate the effects of PMD in DDO-OFDM. We begin with an analysis of the frequency-selective fading caused by first-order PMD. We then estimate the impact of PMD in single-receiver DDO-OFDM using all-order simulations, to find the outage probabilities as a function of SNR penalty. The performances of three frequency allocations are compared, and one new allocation that minimizes the frequency separation between the carrier and the outermost subcarrier is found to be more robust to PMD. We then present an improved DDO-OFDM system that includes polarization diversity [18], [19] and enables a simple implementation of carrier boost [13]. Various configurations are considered, and simulations suggest

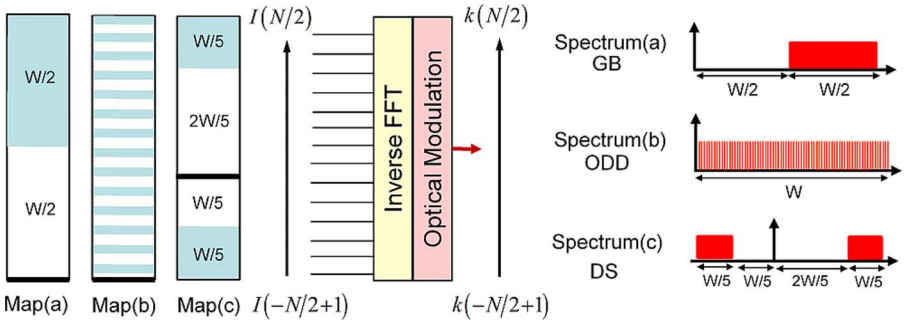

Fig. 2. IFFT mapping and optical spectra. For the maps, white space denotes nulled subcarriers, gray space denotes data carrying subcarriers and the thick black line denotes the virtual carrier. W is twice the Nyquist bandwidth.

that a data rate of 42.7 Gb/s can be achieved within an optical bandwidth of 40 GHz, and with negligible PMD penalties.

This paper is organized as follows. Section II describes the basic DDO-OFDM system and subcarrier allocations. Section III presents an analysis for fading caused by first-order PMD. Section IV estimates PMD penalties. In Section V, we present an improved DDO-OFDM system, and in Section VI, we summarize our findings.

II. System Description

A simple single-receiver DDO-OFDM system is shown in Fig. 1. The quadrature-amplitude-modulated (QAM) symbols are mapped into vectors at the input of the transmitter's inverse fast Fourier transform (IFFT) and then modulated and multiplexed onto orthogonal subcarriers in a single operation. A cyclic prefix is added and the complex baseband can be represented by

$$S(t) = \sum_{i=-\infty}^{i=\infty} \left(\sum_{k=-N/2+1}^{k=N/2} C_{i,k} \prod (t - iT_s) \times \exp\left(j2\pi f_{i,k}(t - iT_s)\right) \right)$$
$$T_s = T_{\mathrm{FFT}} + T_g \tag{1}$$

where $f_{i,k}$ is the frequency of the kth subcarrier in the ith symbol, $C_{i,k} = A_{i,k} + jB_{i,k}$ is the complex QAM mapping, N is the IFFT size, and T_g, T_{FFT}, and T_s are the guard, FFT window, and OFDM symbol times, respectively. The real and imaginary components of (1) are used to drive the I and Q inputs of the optical modulator around their intensity nulls for linear field modulation. This, combined with optical single sideband (OSSB) transmission, allows a one-to-one mapping between subcarriers in the optical and electrical domains. For the ith symbol, the output of the optical modulator in real form is

$$E(t) = \sum_{k=-N/2+1}^{N/2} A'_k \cos\left(2\pi(f_c + f_k)t\right) - B'_k \sin\left(2\pi(f_c + f_k)t\right), \qquad 0 \le t < T \tag{2}$$

where A'_k and B'_k are the upconverted components for the QAM mapping C_k in (1), f_c is the frequency of the optical carrier, and $(f_c + f_k)$ is the frequency of the kth subcarrier. In [14], a direct current (dc) component was added to generate an optical carrier and enable direct detection of the optical OFDM signal. In this paper, the single-receiver investigations will use the technique described in [20], in which a band-edge subcarrier is used as a virtual carrier for more efficient use of the digital-to-analog converter (DAC) bandwidth.

The PMD performance of single-receiver DDO-OFDM with three different subcarrier allocations will be investigated. These allocations are determined by the data mapping at the input of the transmitter IFFT, given by vector $\mathbf{I}$. Three mappings are shown in Fig. 2, along with the their resulting spectra after optical modulation. The index for elements in $\mathbf{I}$ and the corresponding subcarrier outputs k in (1) are the same.

For map (a), the input mapping at the IFFT input is

$$\mathbf{I} = [VC \quad 0_{N/2} \quad I_{N/2-1}] \tag{3}$$

where VC is the input for the virtual carrier, and subscripts refer to the number of elements. Therefore, $0_{N/2}$ is a series of $N/2$ zeroed inputs, and $I_{N/2-1}$ is a series of $N/2 - 1$ information bearing subcarriers. This input mapping leads to a subcarrier allocation with a guardband (GB) and sideband bandwidth of $W/2$. This is shown in spectrum (a) and represents the GB subcarrier allocation [8].

For map (b), the input mapping at the IFFT input is

$$\mathbf{I} = [VC \quad I_1 \quad 0_1 \quad I_1 \quad 0_1 \quad I_1 \ldots I_1]. \tag{4}$$

The IFFT inputs are alternately information bearing and zeroed. This mapping leads to an interleaved subcarrier allocation with a sideband bandwidth of $W/2$ covering an optical bandwidth of W as shown in spectrum (b). At detection, the subcarrier $\times$ subcarrier products fall on the nulled subcarriers [20]. Spectrum (b) represents the interleaved (INT) subcarrier allocation.

For map (c), the input mapping at the IFFT input is

$$\mathbf{I} = [I_{N/5} \quad 0_{N/5} \quad VC \quad 0_{2N/5} \quad I_{N/5-1}]. \tag{5}$$

In this case, the negative $N/5$ and positive $N/5 - 1$ band-edge subcarriers are information bearing. The virtual carrier is offset to achieve a frequency separation of $W/5$ relative to the lower sideband, and $2W/5$ relative to the upper sideband. This is shown in spectrum (c) and represents the double-sided (DS) allocation.

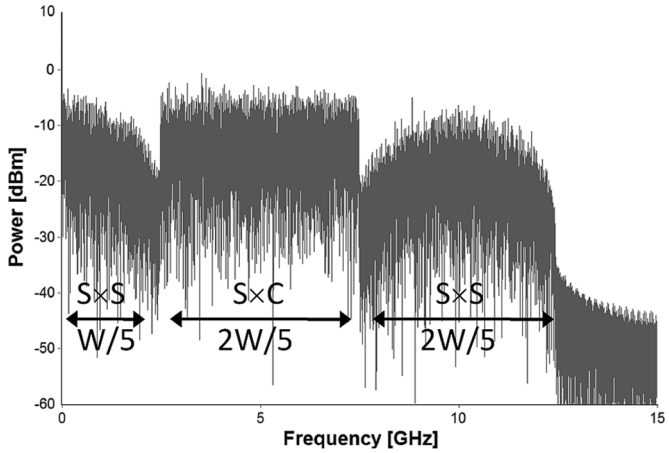

Fig. 3. DS electrical spectrum after detection; $S \times S$ = unwanted subcarrier × subcarrier products; $S \times C$ = wanted subcarrier × carrier products.

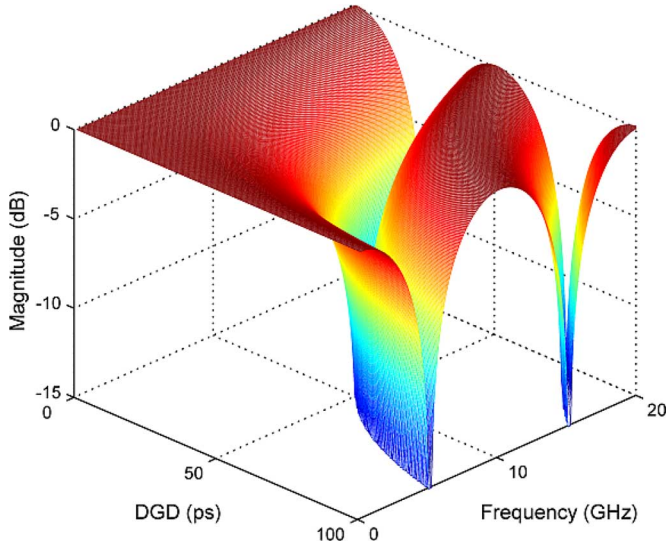

Fig. 4. First-order PMD channel magnitude as a function of DGD and frequency. The input SOP angle $\theta = \pi/4$ for maximum fading.

Upon detection, the upper sideband and the complex conjugate of the lower sideband generate the electrical spectrum in Fig. 3. It is worth noting that only $2W/5$ of the bandwidth for the DS allocation can be information bearing. Therefore, for equal sideband bandwidths between the GB, INT, and DS allocations, the DS allocation requires a 1.2× higher DAC sampling rate and optical bandwidth.

III. PMD Analysis

PMD causes differential group delays (DGDs) and frequency-dependent phase shifts between signal components travelling on each polarization. At detection, the orthogonal contributions add in the electrical domain. If the contributions for a subcarrier are similar in magnitude and out of phase, then deep fading will occur and significantly reduce the electrical SNR in the affected subcarriers [21].

A. First Order PMD

PMD is frequency dependent and can be expressed as a Taylor series expansion about the carrier frequency [22]. The first term represents first-order PMD and is the frequency independent group delay between the two eigenpolarizations. We consider a linearly polarized DDO-OFDM input signal with an input state of polarization (SOP) given by the Jones vector $\hat{p} = (\cos\theta \ \sin\theta)^T$. The angle θ is arbitrary to the eigenpolarization aligned with $\hat{x}$, and determines the power splitting into each mode. The received DDO-OFDM signal in the frequency domain is given by

$$\vec{E}_{out}(\omega) = D(\omega)E_{c,in}(\omega)\hat{p} + D(\omega)E_{s,in}(\omega)\hat{p} \tag{6}$$

where $\vec{E}_{c,in}$ and $\vec{E}_{s,in}$ are the input carrier and sideband terms and $D(\omega)$ describes the DGD between polarizations [23]

$$D(\omega) = \begin{pmatrix} \exp\left(-j(\Delta\tau\omega/2)\right) & 0 \\ 0 & \exp\left(j(\Delta\tau\omega/2)\right) \end{pmatrix}$$

where Δt is the DGD. From (7), the signal at the receiver is given by

$$\vec{E}_{out} = \left(\cos\theta\exp(-j\omega_c\Delta\tau) + \cos\theta\exp(-j\omega_s\Delta\tau)\right)\hat{x} + \left(\sin\theta\exp(j\omega_c\Delta\tau) + \sin\theta\exp(j\omega_s\Delta\tau)\right)\hat{y} \tag{7}$$

where ω_c is the angular frequency of the optical carrier, ω_k is the angular frequency of the kth subcarrier before optical modulation, and $\omega_s = (\omega_c + \omega_k)$. Upon detection, the signal is down-converted to the electrical domain and the channel magnitude is given by

$$|H(\omega_k, \Delta\tau, \theta)| = \left|\cos^2\theta\exp(j\omega_k\Delta\tau) + \sin^2\theta\exp(-j\omega_k\Delta\tau)\right|. \tag{8}$$

The deepest fading occurs when the input signal is split equally into each polarization mode. This occurs for a power splitting ratio $\gamma = 0.5$ where $\gamma = (\cos 2\theta + 1)/2$ and the input SOP angle $\theta = \pi/4$. The channel response (8) becomes

$$|H(f_k, \Delta\tau)| = \left|\cos(\pi f_k\Delta\tau)\right|. \tag{9}$$

The channel magnitude in (9) is a function of DGD and frequency and is plotted in Fig. 4. The signal fading is deep when the subcarrier contributions from each polarization mode add, out-of-phase, in the electrical domain. It is worth noting that the fading is constant for a fixed product of DGD and frequency.

The channel magnitude as a function of frequency and the SOP angle θ

$$|H(f_k, \theta)| = \left|\cos^2\theta\exp(j2\pi f_k\Delta\tau) + \sin^2\theta\exp(-j2\pi f_k\Delta\tau)\right|. \tag{10}$$

The response in (11) is plotted in Fig. 5 for a DGD of 100 ps and shows the impact of the SOP angle θ on the channel response. The fading is minimal for θ, which couples most of the input signal into a single polarization (γ approaching 0 or 1) and

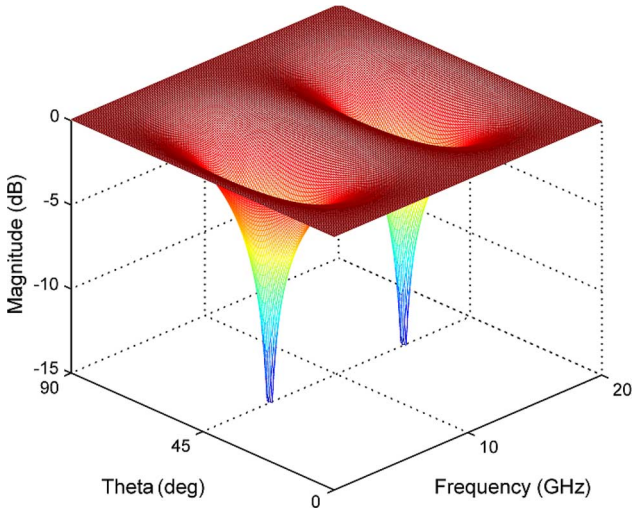

Fig. 5. First-order PMD channel magnitude as a function of input SOP angle and frequency for a DGD of 100 ps.

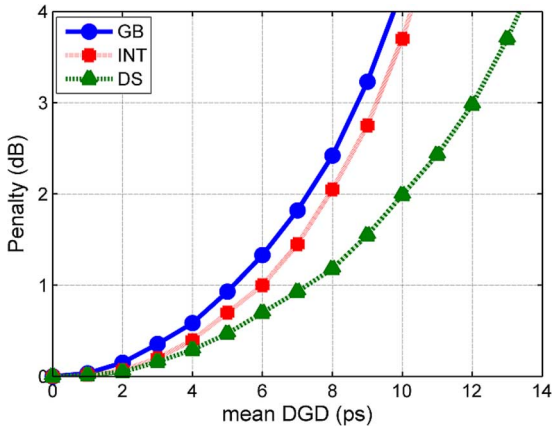

Fig. 6. PMD penalties for the GB, INT, and DS subcarrier allocations using 4-QAM, 5-GHz sideband bandwidth, mean DGD of 0–15 ps, a target BER of 1×10^{-3} at an outage probability of 1×10^{-5}.

increases for θ that couples power evenly into both polarizations (γ approaching 0.5).

IV. Outage Probability

A. Simulation Model

In this section, we investigate the penalties caused by all-order PMD in single-receiver DDO-OFDM for the three subcarrier allocations in Fig. 2. The penalties are found as outage probabilities, defined as the probability that the bit error rate (BER) is exceeded for a fixed SNR penalty. Multiple system configurations were considered and the results help provide guidelines to improve performance for a given link PMD.

The PMD penalties were estimated using Monte Carlo simulations and the stochastic coarse-step PMD model in VPItransmissionMaker. In comparison to analytical methods [21], this method has the advantage of including the higher orders of PMD. However, large numbers of simulations are required to assess the penalties that occur with low probability. To enable the accurate simulation of penalties with probabilities lower than 1×10^{-5}, VPItransmissionMaker includes an option for importance sampling. This technique allows a parameter in the simulation to be modified to bias the probability distribution towards higher DGD levels. The probability distribution can then be corrected by weighting each simulation result with its likelihood ratio. The process is described in detail in [24].

The performances for the three allocations were estimated by running four sets of 10 000 fiber realizations with mean DGDs between 1 and 15 ps, sideband bandwidths of 5 and 10 GHz, and with 4- and 16-QAM subcarrier modulation. The coarse-step model was set to divide the fiber into 50 dithered-length sections with constant birefringence. At the end of each section, the polarization state of the signal was scattered over the Poincaré sphere. The scattering was random for the first simulation set, and biased to correlate the PMD vectors in adjacent fiber sections for the other three sets. The biasing parameter in VPItransmissionMaker is the "correlate scattering factor" and values of 0.2, 0.33, and 0.5 were used.

The detected DDO-OFDM signals were processed in MATLAB. For each fiber realization, the channel response was derived and the additional receiver SNR required to maintain a BER of 1×10^{-3} was calculated. The SNR penalties were quantized to a range of 20 values, or bins, and the frequency of occurrence for each penalty was weighted by its likelihood ratio, and the accumulated occurrences for each bin were recorded. From this distribution of data values, the complementary cumulative distribution was derived and represents the outage probability as a function of receiver SNR penalty. For all simulations: 1) a cyclic prefix size of one eighth of the symbol length was used; 2) the number of possible subcarriers N was 512; 3) operation in the linear regime was assumed, i.e., nonlinear effects were not simulated; and 4) 1600 ps/nm of chromatic dispersion was added. From [25], the variations in mean DGD were assumed to change at a rate that allowed adequate equalizer training.

B. Simulation Results

The results for the three allocations using a 4-QAM, 5-GHz sideband bandwidth and varying mean DGD are shown in Fig. 6. The results show that the DS subcarrier allocation provided the lowest penalties. In the simulations, the fading induced in single-receiver DDO-OFDM could be generalized as having a bandpass characteristic that is symmetrical about the carrier.

The DS allocation reduces the frequency difference between the carrier and the outermost subcarrier for a given bandwidth, as is shown in the optical spectra in Fig. 2 and the electrical spectra in Fig. 7. The ratio between the sideband bandwidth and the maximum carrier-subcarrier frequency difference is 2/3 for the DS allocation, and 1/2 for the GB and INT allocations. The INT allocation performed only marginally better than the GB allocation. The higher average electrical SNR for the INT allocation was largely offset by the shared *bad* subcarriers.

The results for the large number of configurations presented two useful relationships. The first is that the constellation size did not have a significant effect on PMD penalties. For all simulations with the use of 4 or 16 QAM as the only variable, the penalties agreed within a 10% tolerance. This suggests that

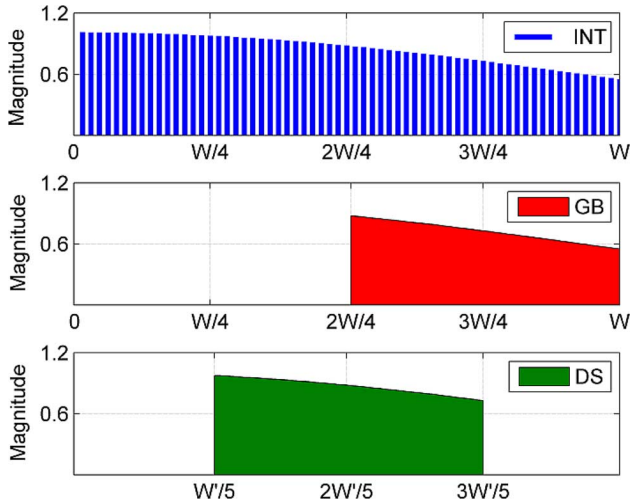

Fig. 7. Detected electrical spectra showing fading for the GB, DS, and INT allocations, for equal sideband bandwidths and for a single random fiber realization. Note the DS allocation requires $1.2 \times W$ for equal sideband as discussed in Section II.

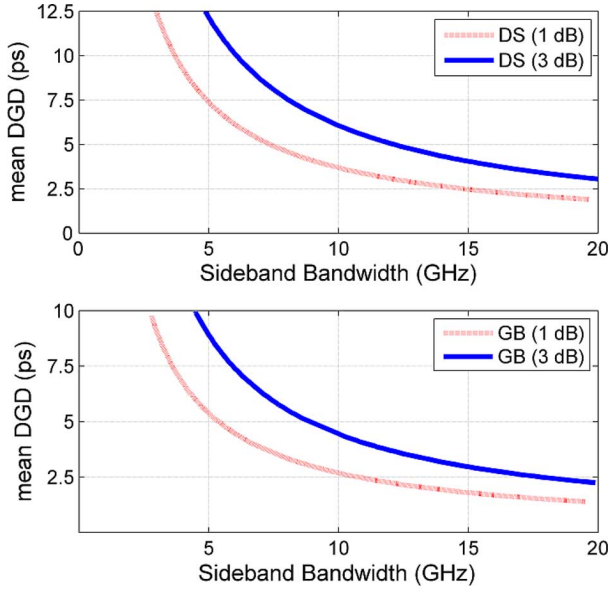

Fig. 8. The left-hand side of the curves show the bandwidth and mean DGD combinations that can maintain a BER of 1×10^{-3} with an outage probability of equal to, or lower than 1×10^{-5} for 1- and 3-dB SNR penalties.

higher order constellations, with higher data rates for a given bandwidth, may be useful in high PMD links if the reduced sensitivity can be accommodated, and if impairments caused by fiber nonlinearities remain negligible. The second relationship is that for a given subcarrier allocation, the PMD penalties for simulations with the same product of mean DGD, and sideband bandwidth agreed within a 5% tolerance. This means that mean DGD and sideband bandwidth can be scaled for a known PMD penalty.

In Fig. 8, the mean DGD and sideband bandwidths were scaled for receiver SNR penalties of 1 and 3 dB for both the GB and DS allocations. The parameter space to the left of these curves shows various combinations of sideband bandwidth and mean DGD that allow a BER of 1×10^{-3} to be maintained, with an outage probability that is equal to, or lower than 1×10^{-5}. These curves apply to both 4- and 16-QAM subcarrier modulation. For typical system optical signal to noise ratios (OSNRs) that would give a BER of 1×10^{-3} for the system in Fig. 1, there is a close relationship between changes in OSNR and resulting changes in the received electrical SNR [26]. Therefore, the 1- and 3-dB SNR penalties can be combined with the OSNR sensitivities in Table I to approximate the total OSNR requirements for a given system configuration. The combination of Fig. 8 and Table I allows the performance of different constellation sizes and sideband bandwidths to be compared for a given link mean DGD, with the assumption that nonlinear impairments remain negligible.

TABLE I
SIMULATED OSNR (dB/0.1 nm) REQUIREMENTS FOR BER $= 1 \times 10^{-3}$

Sideband Bandwidth (GHz)	QAM	Bit Rate (Gbit/s)	OSNR (dB/0.1 nm) DB	OSNR (dB/0.1 nm) GB
5	4	10	11.1	11.3
10	4	20	14.2	14.4
5	16	20	17.6	17.8
10	16	40	20.7	20.8

V. POLARIZATION DIVERSITY

A. System Description

In this section, we introduce a DDO-OFDM receiver topology that enables high data rates in links with high PMD. The topology of the system is presented in Fig. 9 and enables increased signal bandwidths for high data rates using low-order subcarrier modulation for improved sensitivity. The transmitter uses a radio frequency (RF) mixer with the complex baseband to generate both a *real* electrical signal and a frequency guard band [8], [14]. This allows most of the subcarriers to carry data and as a result reduces the DAC sampling rate requirements compared with the topology in Fig. 1.

The electrical signal then drives a single-input optical modulator and an optical filter is used to suppress the lower sideband. The optical modulator is biased to generate an optical carrier of approximately equal power to the sideband. For the ith symbol, the output of the optical modulator in real form is similar to (2)

$$e(t) = A_0 \cos(2\pi f_0 t) + \sum_{k=-N/2+1}^{N/2} A_k \cos\left(2\pi(f_0 + f_{k,RF})t\right) - B_k \sin\left(2\pi(f_0 + f_{k,RF})t\right), \qquad 0 \le t < T \quad (11)$$

where A_0 is the carrier amplitude, $f_{k,RF}$ are the subcarrier frequencies after electrical up-conversion, and $C_k = A_k + jB_k$ is the complex QAM mapping. Further reductions in DAC sampling rate requirements can be gained by mixing multiple baseband outputs with multiple RF carriers to create adjacent subbands [10], [11].

To recover the wide-bandwidth optical signal, the receiver incorporates both polarization diversity and carrier boost [13]. The receiver topology can be described as follows. The received signal is split into two branches. The signal in the upper branch (A) is filtered to reject the carrier and to provide amplified spontaneous emission (ASE) filtering. The sideband signal at both

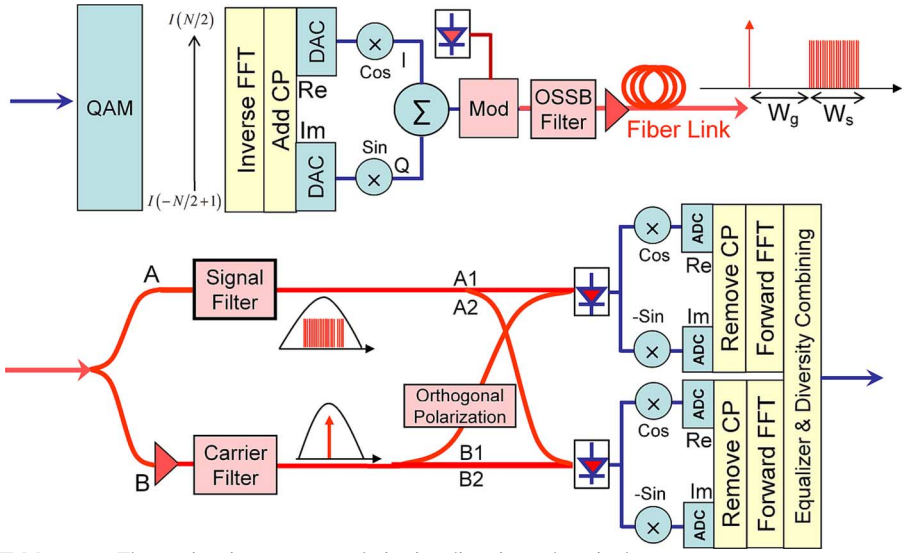

Fig. 9. Improved DDO-OFDM system. The receiver incorporates polarization diversity and carrier boost.

photodiodes (A1 and A2) for first-order PMD can be derived simply from (8)

$$\vec{E}_{s,\mathrm{out}} = \frac{1}{\sqrt{2}}\left(\left(\cos\theta \exp(-j\omega_s \Delta\tau)\right)\hat{x} + \left(\sin\theta \exp(j\omega_s \Delta\tau)\right)\hat{y}\right). \tag{12}$$

The signal in the lower branch (B) is boosted with an optical amplifier and filtered to isolate the carrier. For diversity reception, orthogonal carrier polarizations are required. In [19], the carrier was filtered and orthogonal polarizations were generated using a circulator, a fiber Bragg grating, and a Faraday rotator mirror for self-polarization diversity. Alternate configurations could use a polarization beam splitter and dynamic polarization control. For first-order PMD, the two orthogonally polarized carrier signals can be represented by

$$\vec{E}_{c1,\mathrm{out}} = \frac{G}{\sqrt{2}}\left(\left(\cos\theta \exp(-j\omega_c \Delta\tau)\right)\hat{x} + \left(\sin\theta \exp(j\omega_c \Delta\tau)\right)\hat{y}\right) \tag{13}$$

$$\vec{E}_{c2,\mathrm{out}} = \frac{G}{\sqrt{2}}\left(-\left(\sin(\theta) \exp(-j\omega_c \Delta\tau)\right)\hat{x} + \left(\cos(\theta) \exp(j\omega_c \Delta\tau)\right)\hat{y}\right) \tag{14}$$

where G is the amplifier gain and the carrier signals $\vec{E}_{c1,\mathrm{out}}$ and $\vec{E}_{c2,\mathrm{out}}$ mix with the sideband signals at the upper and lower photodiodes, respectively. The signals are then detected, down-converted, sampled, and demodulated. The frequency-domain signals from both branches are equalized and combined using maximum ratio combining [18]. The estimate for each subcarrier k in the ith symbol is given by

$$\tilde{R}_k = \frac{Y_{k,u}\tilde{H}^*_{k,u} + Y_{k,v}\tilde{H}^*_{k,v}}{|\tilde{H}_{k,u}|^2 + |\tilde{H}_{k,v}|^2} \tag{15}$$

where $\tilde{R}_k$ is the estimated signal after diversity combining, u and v are the carrier axis at each branch, $Y_{k,u}$ and $Y_{k,v}$ are the received signals from each photodiode, $\tilde{H}_{k,u}$ and $\tilde{H}_{k,v}$ are the channel estimates for each branch, and $(^*)$ is the complex conjugate operator. In the absence of polarization-dependent loss (PDL), and with uncorrelated noise on each polarization, DGD up to the length of the CP can be compensated for without penalty.

B. Simulation Details

Three properties of the receiver performance were explored. The first was the use of carrier boost to increase sensitivity, the second was the use of carrier boost to increase spectral efficiency, and the third was PMD performance. All of the simulations used a sideband bandwidth of 25 GHz for a raw data rate of 50 and 42.7 Gb/s after overheads. The symbol size and cyclic prefix were 1024 and 128 samples, respectively.

For the sensitivity simulations, equal frequency GB and sideband bandwidths were used ($W_g = W_s$ in Fig. 9) so with a 37.5-GHz RF carrier, the optical spectrum was 25–50 GHz relative to the optical carrier. For the simulations with the halved frequency GB ($W_g = W_s/2$ in Fig. 9), a 25-GHz RF carrier was used for an optical spectrum of 12.5–37.5 GHz relative to the optical carrier. To filter the carrier, a 12.5-GHz optical filter was used with a fourth-order rolloff, a 3-dB insertion loss, and a stop band suppression of 45 dB. A 30-GHz fourth-order optical filter was used for ASE suppression. The carrier boost amplifier had a noise figure of 4 dB.

The receiver in Fig. 9 needs to have similar path lengths for the carrier and signal at detection. If path lengths are greater than 2 m, the high tolerance to laser phase noise is degraded.

C. Carrier Boost: Sensitivity

For conventional DDO-OFDM, the ratio of transmitted carrier and sideband power is approximately 1 : 1 for optimal sensitivity. However, with the receiver in Fig. 9, the carrier power can be reduced at transmission and then boosted at the receiver to maintain a 1 : 1 power ratio at the photodiode for a potential 3-dB sensitivity increase. Simulations were run for various levels of optical carrier suppression, however Fig. 10 shows that only a 0.2-dB improvement was realized with the 12.5-GHz carrier filter. This is because the filter width allows too much noise to be amplified with the carrier and mixed with the signal. In comparison, a 1-GHz carrier filter allowed a 1.5-dB improvement in sensitivity with a carrier suppression of 4 dB or more.

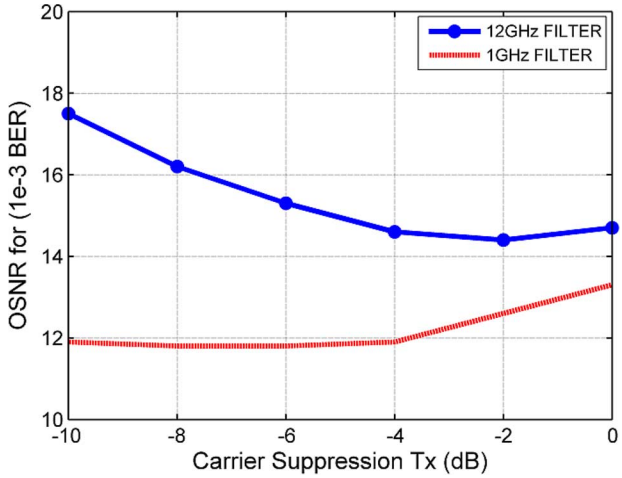

Fig. 10. Sensitivity change by varying the optical carrier level at transmission and compensating with carrier boost at the receiver for a constant 1 : 1 carrier to signal power ratio at the photodiode. System has the same frequency guard and sideband bandwidth.

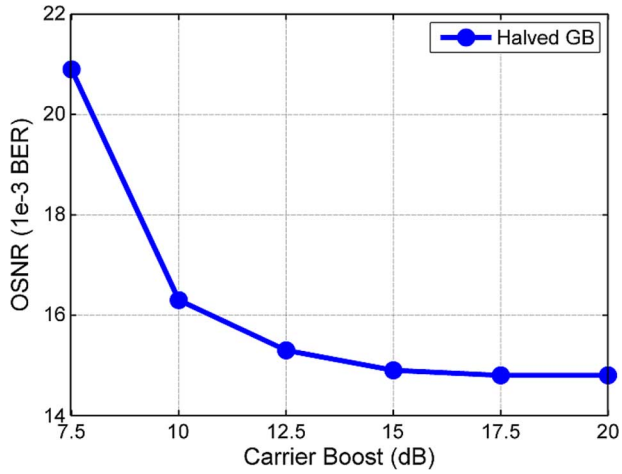

Fig. 11. OSNR (dB/0.1 nm) versus carrier boost for the system with a halved frequency guard bandwidth and 12.5-GHz carrier filter.

D. Carrier Boost: Spectral Efficiency

The frequency guard bandwidth was halved to increase spectral efficiency and to enable a data rate of 42.7 Gb/s within an optical bandwidth of 40 GHz. However, by halving the frequency guard band, some sideband $\times$ sideband products fall inband and cause significant impairments. The use of carrier boost in the receiver can reduce these impairments by increasing the wanted carrier $\times$ sideband products relative to the unwanted sideband $\times$ sideband products [13]. Simulations were run with the frequency GB bandwidth halved to 12.5 GHz which allows an increase in spectral efficiency of 33%. A 12.5-GHz carrier filter was used with boost levels between 7.5 and 20 dB. The results are shown in Fig. 11 and with boost levels of 15 dB or more, the receiver can effectively mitigate the inband distortion caused by the halved frequency guard bandwidth.

E. PMD Performance

The PMD penalties for the diversity receiver using both frequency guard bandwidths were approximated using all-order

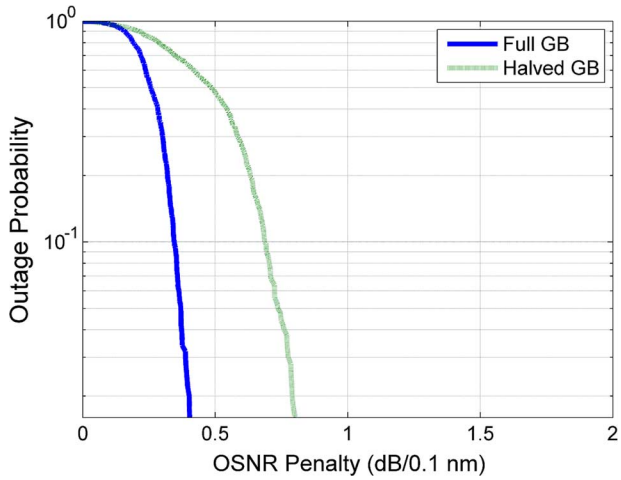

Fig. 12. PMD performance with 25-ps mean DGD. Results for both the normal and halved frequency GB given.

Monte Carlo simulations with a mean DGD of 25 ps. Five hundred fiber realizations and an orthogonal carrier polarization were generated for each run. The results for the diversity receiver are presented in Fig. 12 as an outage probability as a function of OSNR penalty. The penalties are low and the steep gradient for the curves show the effectiveness of polarization diversity reception in mitigating all-order PMD as reported in [18], [19].

VI. Conclusion

The impact of PMD in DDO-OFDM has been examined by using all-order PMD simulations to find the outage probability as a function of receiver SNR penalty for a variety of system configurations. The frequency-domain fading caused by first-order PMD in single-receiver DDO-OFDM was examined analytically, and the impact of all-order PMD was then estimated via simulation over a range of mean DGD values.

For high data rate transmission in high PMD links, a new receiver topology has been introduced that incorporates polarization diversity and carrier boost. Simulations have shown that carrier boost can mitigate the inband distortion caused by a reduced frequency guard bandwidth. A 33% increase in spectral efficiency was realized and a data rate of 42.7 Gb/s was simulated with 4-QAM subcarrier modulation, an optical bandwidth of 40 GHz, and with a sensitivity of 14.8 dB. The polarization diverse receiver has been shown to reduce PMD penalties to very low levels.

Acknowledgment

The authors would like to thank L. Du at Monash University for helpful discussions and VPIphotonics, Holmdel, NJ, for the use of their simulator VPItransmissionMaker V7.6.

References

[1] H.-M. Bae, J. B. Ashbrook, J. Park, N. R. Shanbhag, A. C. Singer, and S. Chopra, "An MLSE receiver for electronic dispersion compensation of OC-192 fiber links," *IEEE J. Solid-State Circuits*, vol. 41, no. 11, pp. 2541–2553, Nov. 2006.

[2] F. Buchali and H. Bulow, "Adaptive PMD compensation by electrical and optical techniques," *J. Lightw. Technol.*, vol. 22, no. 4, pp. 1116–1126, Apr. 2004.
[3] T. Foggi, E. Forestieri, G. Colavolpe, and G. Prati, "Maximum likelihood sequence detection with closed-form metrics in OOK optical systems impaired by GVD and PMD," *J. Lightw. Technol.*, vol. 24, no. 8, pp. 3073–3087, Aug. 2006.
[4] T. Foggi, G. Colavolpe, E. Forestieri, and G. Prati, "Channel estimation algorithms for MLSD in optical communication systems," *Photon. Technol. Lett.*, vol. 18, pp. 1984–1986, Oct. 2006.
[5] O. E. Agazzi, M. R. Hueda, H. S. Carrer, and D. E. Crivelli, "Maximum-likelihood sequence estimation in dispersive optical channels," *J. Lightw. Technol.*, vol. 23, no. 2, pp. 749–763, Feb. 2005.
[6] H. Bulow, "Electronic dispersion compensation," presented at the Opt. Fiber Commun. Conf., Anaheim, CA, 2007, paper OMG5, unpublished.
[7] G. Colavolpe, T. Foggi, E. Forestieri, and G. Prati, "Multilevel optical systems with MLSD receivers insensitive to GVD and PMD," *J. Lightw. Technol.*, vol. 26, no. 10, pp. 1263–1273, May 2008.
[8] A. J. Lowery and J. Armstrong, "Orthogonal-frequency-division multiplexing for dispersion compensation of long-haul optical systems," *Opt. Exp.*, vol. 14, no. 6, pp. 2079–2084, Mar. 2006.
[9] W. Shieh and C. Athaudage, "Coherent orthogonal frequency division multiplexing," *Electron. Lett.*, vol. 42, no. 10, pp. 587–589, May 2006.
[10] S. L. Jansen, I. Morita, and H. Tanaka, "10 × 121.9-Gb/s PDM-OFDM transmission with 2-b/s/Hz spectral efficiency over 1,000 km of SSMF," presented at the Opt. Fiber Commun. Conf., San Diego, CA, 2008, paper PDP2, unpublished.
[11] Q. Yang, Y. Ma, and W. Shieh, "107 Gb/s coherent optical OFDM reception using orthogonal band multiplexing," presented at the Opt. Fiber Commun. Conf., San Diego, CA, 2008, paper PDP7, unpublished.
[12] S. L. Jansen, I. Morita, T. C. W. Schenk, N. Takeda, and H. Tanaka, "Coherent optical 25.8-Gb/s OFDM transmission over 4160-km SSMF," *J. Lightw. Technol.*, vol. 26, no. 1, pp. 6–15, Jan. 2008.
[13] A. J. Lowery, "Improving sensitivity and spectral efficiency in direct-detection optical OFDM systems," presented at the Opt. Fiber Commun. Conf., San Diego, CA, 2008, paper OMM4, unpublished.
[14] B. J. C. Schmidt, A. J. Lowery, and J. Armstrong, "Experimental demonstrations of electronic dispersion compensation for long-haul transmission using direct-detection optical OFDM," *J. Lightw. Technol.*, vol. 26, no. 1, pp. 196–203, Jan. 2008.
[15] C. Xie, "Polarization-mode-dispersion impairments and mitigation in ultra-high speed transmission," in *IEEE/LEOS Summer Top. Meet.*, 2007, pp. 244–245.
[16] N. Cvijetic, L. Xu, and T. Wang, "Adaptive PMD compensation using OFDM in long-haul 10 Gb/s DWDM systems," presented at the Opt. Fiber Commun. Conf., Anaheim, CA, 2007, paper OTuA5, unpublished.
[17] I. B. Djordjevic, "PMD compensation in fiber-optic communication systems with direct detection using LDPC-coded OFDM," *Opt. Exp.*, vol. 15, no. 7, pp. 3692–3701, Apr. 2007.
[18] M. Mayrock and H. Haunstein, "PMD tolerant direct-detection optical OFDM system," presented at the Proc. Eur. Conf. Opt. Commun., Berlin, Germany, 2007, paper Tu. 5.2.5, unpublished.
[19] C. Xie, "PMD insensitive direct-detection optical OFDM systems using self-polarization diversity," presented at the Opt. Fiber Commun. Conf., San Diego, CA, 2008, paper OMM2, unpublished.
[20] W.-R. Peng, X. Wu, V. R. Arbab, B. Shamee, L. C. Christen, J. Y. Yang, K. M. Feng, A. E. Willner, and S. Chi, "Experimental demonstration of a coherently modulated and directly detected optical OFDM system using an RF-tone insertion," presented at the Opt. Fiber Commun. Conf., San Diego, CA, 2008, paper OMU2, unpublished.
[21] N. Cvijetic, S. G. Wilson, and D. Qian, "System outage probability due to PMD in high-speed optical OFDM transmission," *J. Lightw. Technol.*, vol. 26, no. 14, pp. 2118–2127, Jul. 2008.
[22] H. Kogelnik, R. M. Jopson, and L. E. Nelson, "Polarization mode dispersion," in *Optical Fiber Telecommunications*, I. P. Kaminow and T. Li, Eds. San Diego, CA: Academic, 2002, vol. IVB, pp. 725–861.
[23] F. Bruyere, "Impact of first- and second-order PMD in optical digital transmission systems," *Opt. Fiber Technol.*, vol. 2, pp. 269–80, 1996.
[24] G. Biondini, W. L. Kath, and C. R. Menyuk, "Importance sampling for polarization-mode dispersion," *Photon. Technol. Lett.*, vol. 14, pp. 310–312, Feb. 2002.
[25] O. Karlsson, J. Brentel, and P. A. Andrekson, "Long-term measurement of PMD and polarization drift in installed fibers," *J. Lightw. Technol.*, vol. 18, no. 7, pp. 941–51, Jul. 2000.
[26] A. J. Lowery, "Amplified-spontaneous noise limit of optical OFDM lightwave systems," *Opt. Exp.*, vol. 16, pp. 860–865, Jan. 2008.

Brendon J. C. Schmidt received the B.Eng. degree (first class honors) in electrical and computer systems engineering from Monash University, Melbourne, Vic., Australia, in 2006, where he is currently working towards the Ph.D. degree in the field of OFDM in optical communications.

His research interests include OFDM in optical applications.

Arthur James Lowery (M'91–SM'96–F'09) was born in Yorkshire, U.K., in 1961. He received the B.Sc. degree (first class) in applied physics from the University of Durham, Durham, U.K., in 1983 and the Ph.D. degree in electrical and electronic engineering from the University of Nottingham, Nottigham, U.K., in 1988.

In 1983–1984, he worked at Marconi Radar Systems Ltd., U.K. In 1984, he joined the University of Nottingham as a Lecturer and pioneered time-domain field modeling of semiconductor lasers as the transmission-line laser model. In 1990, he became a Senior Lecturer at the Photonics Research Laboratory, University of Melbourne, Melbourne, Vic., Australia. After working on photonic-CAD, packet switching and laser ranging, he was promoted to Associate Professor and Reader in 1993. He continued to develop novel time-domain simulation techniques and to lead collaborative research as a Fellow of the Australian Photonics Cooperative Research Centre. In 1996, he cofounded Virtual Photonics Pty, Ltd., with P. Gurney. In 1995, Optoelectronic, Photonic and Advanced Laser Simulator (OPALS) was released, followed by Gigabit Optical Link Designer (GOLD). Virtual Photonics merged with BNeD (Berlin, Germany) in 1998, and he became a CTO, leading the development of VPI's physical-level photonic design automation tools such as VPItransmissionMaker and VPIcomponentMaker, which are widely used in industry and academia for development, research, and teaching. In 2004, he was appointed Professor of Electrical and Computer Systems Engineering at Monash University, Melbourne, Vic., Australia, where he works on active photonic circuits and the applications of photonic technology, particularly optical-OFDM. In 2008, he founded Ofidium Pty, Ltd., to commercialize the optical OFDM developed at Monash University. He has published more than 200 papers and four book chapters on the simulation of photonic devices and circuits and photonic applications such as mode-locking, packet switching, transmission systems and high-speed photonic circuits.

Prof. Lowery is a Fellow of the Institution of Engineering and Technology (IET) and the Australian Academy of Technological Sciences and Engineering (ATSE).

Jean Armstrong (M'89–SM'06) received the B.Sc. degree (first class honors) in electrical engineering from the University of Edinburgh, Edinburgh, Scotland, in 1974, the M.Sc. degree in digital techniques from Heriot-Watt University, Edinburgh, Scotland, in 1980, and the Ph.D. degree in digital communications from Monash University, Melbourne, Vic., Australia, in 1993.

From 1974 to 1977, she was a Design Engineer at Hewlett-Packard Ltd., Scotland. In 1977, she was appointed Lecturer in Electrical Engineering at the University of Melbourne, Melbourne, Vic., Australia. Since 1977, she has held a range of academic positions at the University of Melbourne, Monash University, and La Trobe University. She is currently a Professor at Monash University. Her research interests include digital communications, engineering education, and women in engineering. She has published over 100 papers including over 70 on aspects of OFDM. Her work on OFDM has also led to a number of patents.

Dr. Armstrong is a Fellow of the Institution of Engineers Australia. In June 2006, she and A. Lowery were awarded the Peter Doherty Prize for Innovation for their work on optical OFDM.